2024 IEEE International Conference on Robotics and Automation (ICRA 2024)
May 13-17, 2024. Yokohama, Japan

Constrained Nonlinear Disturbance Observer for Robotic Systems

Ji Wan Han[1], Daehyung Park[2], and Min Jun Kim[1]

Abstract— **Disturbance observer (DOB) is a well-known two-loop control structure that imparts robustness to a controller with a simple implementation. As a nonlinear DOB for the robotic systems, we proposed so-called nonlinear robust internal-loop compensator (NRIC) framework in our previous work. In this paper, we further extend the NRIC in such a way that an optimization scheme can be embedded in the control structure. The proposed method is called constrained NRIC (C-NRIC), because the optimization allows us to impose constraints, by which a controller acquires additional properties. As a particular use case of the C-NRIC framework, we design contact-responsive motion controllers that enables a robot to react to unknown interactions while accurately tracking the desired trajectory in free motion. The effectiveness of such designs is validated through the real-world experiments.**

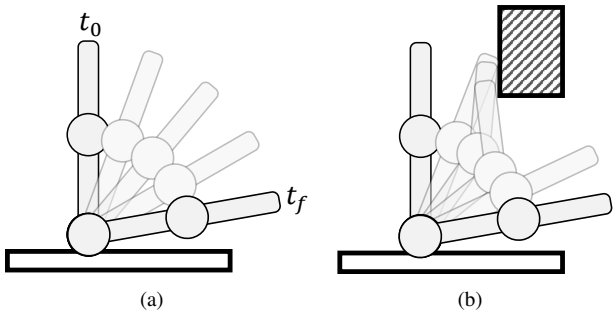

Fig. 1. A design example using the proposed method. A robot can (a) accurately track the desired trajectory in free motion, (b) while reacting to unknown interaction forces.

I. Introduction

As the robots are expected to follow the user's control command accurately, robust control has been one of the most classical and fundamental research topics in the robotics field. Therefore, a number of robust control methods have been proposed in literature; e.g., sliding mode control [1], [2], adaptive methods [3], [4], $\mathcal{H}_\infty$ optimal control [5], [6], and passivity-based methods [7], [8]. As will be introduced shortly, in this paper, we focus on the two-loop structures which are another interesting branch of robust control [9].

However, despite the fact that the real world problems are subject to constraints, it is often not clear how to incorporate them into the aforementioned robust control methods. Although there were attempts to include certain types of constraints like input constraints [10], [11], general extension is still an open question.

In contrast, optimization-based control frameworks such as model predictive control (MPC) and control barrier function (CBF) can naturally include constraints in the formulation. MPC framework optimizes a trajectory of inputs and states over the future horizon, and has been employed in diverse settings; e.g., robust control [12], [13], robot planning with constraints [14], [15], and nonlinear extensions for robot control [16], [17]. Compared to the MPC, a standard setting of the CBF prevents the system from entering unsafe states at the current step, rather than predicting the future horizon [18], [19]. Naturally, CBF is often combined with safety of robots [20]. Hence, It should be pointed out that MPC and CBF are versatile due to the optimization-based formulation.

This work was supported by the National Research Foundation of Korea (NRF) grant funded by the Korea government (MSIT) No. 2021R1C1C1005232, and No. 2021R1A4A3032834.

[1]J. W. Han and M. J. Kim are with the School of Electrical Engineering, and [2]D. Park is with the School of Computing, Korea Advanced Institute of Science and Technology, Daejeon, Republic of Korea. E-mail: {jw.han, daehyung, minjun.kim}@kaist.ac.kr

In this paper, on the other hand, we propose a novel control framework in which optimization can be embedded in a two-loop control structure. Disturbance observer (DOB) is probably the most widely used two-loop control technique, especially for linear systems [21]–[23]. The DOB is known for its robustness against unknown disturbances with a very simple implementation. Another two-loop control structure called robust internal-loop compensator (RIC) is a notable variant of the DOB [24]. RIC is essentially equivalent to the DOB, but it provides a new interpretation that leads us to nonlinear extension called Nonlinear RIC (NRIC) framework, which is a class of nonlinear DOB [25].

Mathematical formulation of the NRIC framework contains two systems; real and nominal robots. Roughly speaking, the nominal robot is simulated in the control computer, providing the nominal signal that the real robot should follow. In the original NRIC framework, a proportional-integral-derivative (PID) and proportional-derivative (PD) controllers are used to make the real robot follow the nominal signals, while guaranteeing the robustness in the sense of nonlinear $\mathcal{H}_\infty$ optimality [25]. Several applications of the NRIC framework are presented in [19], [26]–[28].

This paper presents a method that imposes constraints on the NRIC framework which is a particular type of nonlinear DOBs, by embedding an optimization scheme in the control loop. This method will be called Constrained NRIC (C-NRIC). Since the NRIC framework includes real and nominal robots, the number of states representing the entire system becomes double. Compared to the standard optimization-based frameworks, the proposed method may provide increased flexibility as there exist more states.

As an interesting consequence of such flexibility, we present control designs with which a robot tracks the desired trajectory accurately in free motion, while reacting to

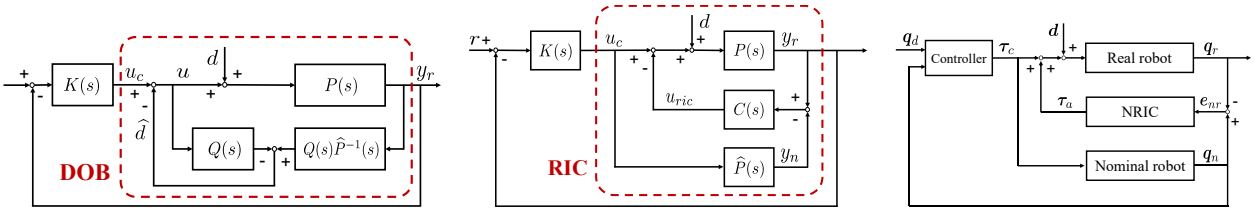

(a) (b) (c)

Fig. 2. (a) DOB structure. (b) RIC structure as a variant of the DOB. (c) NRIC framework which is a nonlinear extension of the DOB through RIC.

unknown external interactions; this will be called contact-responsive motion controller in this paper. In fact, a recent study [28] also proposed a specific control design that can achieve contact-responsiveness, as a particular application of the NRIC. Compared to [28], we present a *framework* that allows us to include optimization in the NRIC structure. With properly designed constraints and objectives, the resulting controller can acquire additional properties. For example, the robot can become more responsive, even with fragile objects like eggs, as demonstrated in our experiments.

The rest of this paper is organized as follows. In Section II, we present a review of the DOB and its nonlinear extension, i.e., NRIC. We proceed to present the proposed C-NRIC framework in Section III, with its theoretical derivation in Section IV. Experimental validations are presented in Section V, and the conclusion is made in Section VI.

II. Background

A. Disturbance observer (DOB)

Disturbance observer (DOB) shown in Fig. 2(a) is a well-known two-loop structure that impart additional robustness to controllers designed for nominal systems. Suppose that there exists a stabilizing controller $K(s)$ for a nominal system. With some algebraic calculation, it is straightforward to see

$$\widehat{d} = \frac{Q(s)\widehat{P}^{-1}(s)P(s)}{\mathcal{X}(s)}d + \frac{Q(s)(\widehat{P}^{-1}(s)P(s)-1)}{\mathcal{X}(s)}u_c, \quad (1)$$

where $\mathcal{X}(s) = (1-Q(s)) + Q(s)\widehat{P}^{-1}(s)P(s)$. $P(s)$ and $\widehat{P}(s)$ are real and nominal plants, respectively. When $Q(s)$ is designed as a low-pass filter, it is easy to see that $y_r = \widehat{P}(s)u_c$ when $Q(s) \simeq 1$. Namely, the system behaves like a disturbance-free nominal system in a low-frequency operating range.

One disadvantage of the DOB is that, in principle, it can be applied only to linear systems because the analysis is based on the transfer functions. Although nonlinear extensions of DOB have been proposed in literature [29], [30], generalization to multi-dimensional robotic systems is not clear. In robotics community, a momentum-based formulation is widely used [26], [31], [32]. However, extension to high-order estimation/compensation is not clear.

B. Robust internal-loop compensator (RIC)

RIC shown in Fig. 2(b) is a variant of DOB. Indeed, one can easily derive the equivalence between RIC and DOB with $Q(s) = \widehat{P}(s)C(s)/\left(1+\widehat{P}(s)C(s)\right)$.

An advantage of RIC is in its interpretation. First, the RIC defines a nominal plant, which is a copy of the real plant. By simulating the nominal plant, the nominal behavior y_n can be obtained, and it is compared with the actual response y_r. Finally, the difference between the real plant and nominal plant $e_{nr} = y_n - y_r$ is attenuated using $C(s)$. As a result, the real behavior y_r follows the nominal one y_n.

Notice that, unlike the DOB structure, RIC does not include inverse of the system model. More specifically, Fig. 2(a) contains $\widehat{P}^{-1}(s)$, whereas Fig. 2(b) runs simulation to obtain nominal signal y_n through $\widehat{P}(s)$. This leads to the nonlinear extension of RIC structure, as introduced in the following.

C. Nonlinear RIC (NRIC)

The NRIC framework is a nonlinear DOB in the sense that the controlled robot behaves like a disturbance-free nominal system. As shown in Fig. 2(c), the structure of NRIC is almost the same as that of RIC, except that (i) the systems are multi-dimensional and nonlinear, and (ii) the nominal signals are fed back into the controller. This paper considers the following PD-type auxiliary input

$$\boldsymbol{\tau}_a = \left(\boldsymbol{L} + \frac{1}{\gamma^2}\boldsymbol{I}\right)(\dot{\boldsymbol{e}}_{nr} + \boldsymbol{L}_p\boldsymbol{e}_{nr}), \quad (2)$$

where $\gamma > 0$ is a control gain. $\boldsymbol{L}$, $\boldsymbol{L}_p$ are diagonal gain matrices, and $\boldsymbol{I}$ is an identity matrix. $\boldsymbol{q}_n$ is the nominal signal, $\boldsymbol{q}_r$ is the real signal measured from the real robot, and $\boldsymbol{e}_{nr} = \boldsymbol{q}_n - \boldsymbol{q}_r$ is the difference between them.

With this setup, [25] proved that the entire system is disturbance input-to-state stable (ISS) when the controller is designed to satisfy asymptotic stability for the equilibrium of interest. In other words, as long as the disturbance input is bounded, boundedness of the state trajectory is guaranteed.

D. Quadratic programming (QP)

In this paper we consider the quadratic programming (QP) problem given by

$$\min_{\boldsymbol{x}} \quad \frac{1}{2}\|\boldsymbol{x}-\bar{\boldsymbol{x}}\|_{\boldsymbol{Q}}^2 \quad (3)$$

$$\text{subject to} \quad \boldsymbol{G}\boldsymbol{x} \le \boldsymbol{h}, \quad (4)$$

where $\|\cdot\|_{\boldsymbol{Q}}^2 = (\cdot)^T\boldsymbol{Q}(\cdot)$ is the $\boldsymbol{Q}$-weighted norm. $\boldsymbol{Q} \in \mathbb{R}^{n\times n}$ defines the non-negative quadratic objective function for a decision variable $\boldsymbol{x} \in \mathbb{R}^n$ with a constant vector $\bar{\boldsymbol{x}} \in \mathbb{R}^n$. Inequality constraint (4) is defined component-wise with $\boldsymbol{G} \in \mathbb{R}^{m\times n}$ and $\boldsymbol{h} \in \mathbb{R}^m$.

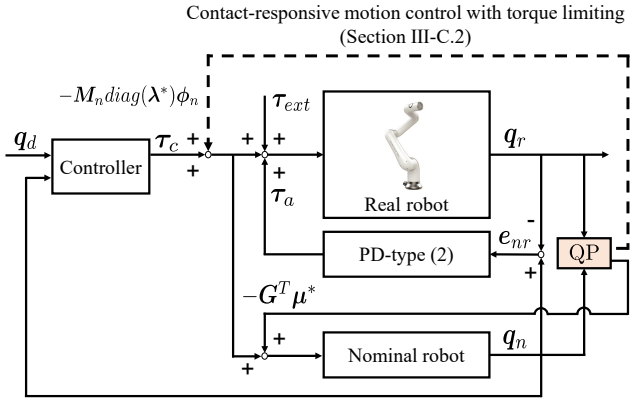

Fig. 3. The proposed C-NRIC framework that can impose constraints on the NRIC framework.

When there exists a strictly feasible $\boldsymbol{x}$,[1] the optimization problem (3)-(4) can be solved by solving the following Karush-Kuhn-Tucker (KKT) conditions [33]

$$\boldsymbol{Q}(\boldsymbol{x}^* - \bar{\boldsymbol{x}}) + \boldsymbol{G}^T\boldsymbol{\mu}^* = \boldsymbol{0}, \tag{5}$$

$$diag(\boldsymbol{\mu}^*)(\boldsymbol{G}\boldsymbol{x}^* - \boldsymbol{h}) = \boldsymbol{0}, \tag{6}$$

$$\boldsymbol{\mu}^* \geq \boldsymbol{0}, \tag{7}$$

$$\boldsymbol{G}\boldsymbol{x}^* - \boldsymbol{h} \leq \boldsymbol{0}, \tag{8}$$

where superscript $*$ represents the optimal value, $\boldsymbol{\mu}$ is the Lagrange multiplier, and (5) is called stationarity condition.

III. Constrained NRIC (C-NRIC) Framework

In this section, we propose C-NRIC framework that can impose constraints on the NRIC which is a nonlinear DOB. Furthermore, as an application of the C-NRIC framework, we present a contact-responsive motion controller that allows the robot to react to unknown interaction while accurately tracking the desired trajectory in free motion (Fig. 1).

Recall that the NRIC framework makes the real robot follow the nominal signal obtained by simulating the nominal system in the control computer. Therefore, by enforcing that the nominal signal does not deviate too much from the real robot, it is possible to design contact-responsive motion controllers. Technically speaking, this can be formulated as a constraint on the state related to $\boldsymbol{e}_{nr}$, as will be introduced in Section III-C.

A. Modeling

The structure of C-NRIC framework is shown in Fig. 3. As stated in Section II-C, in principle, any stabilizing controller can be used for τ_c. In this paper, the following computed torque control, which exponentially stabilizes the equilibrium of interest, is used for simplicity.

$$\boldsymbol{\tau}_c^{CTC} = \widehat{\boldsymbol{M}}_n(\ddot{\boldsymbol{q}}_d \underbrace{-\boldsymbol{k}_v\dot{\boldsymbol{e}}_{nd} - \boldsymbol{k}_p\boldsymbol{e}_{nd}}_{=\boldsymbol{\phi}_n}) + \widehat{\boldsymbol{C}}_n\dot{\boldsymbol{q}}_n + \widehat{\boldsymbol{g}}_n, \tag{9}$$

where $\boldsymbol{e}_{nd} = \boldsymbol{q}_n - \boldsymbol{q}_d$ with the desired trajectory $\boldsymbol{q}_d$. $\boldsymbol{k}_p, \boldsymbol{k}_v$ are positive control gains, and $\boldsymbol{\phi}_n$ is defined for later convenience. $\boldsymbol{M}$, $\boldsymbol{C}$, and $\boldsymbol{g}$ represent the inertia matrix, Coriolis/centrifugal matrix, and gravity vector, respectively. $(\cdot)_n$ is a notation indicating that $(\cdot)$ is a function of nominal signals; e.g., $\boldsymbol{M}_n = \boldsymbol{M}(\boldsymbol{q}_n)$ and $\boldsymbol{C}_n = \boldsymbol{C}(\boldsymbol{q}_n, \dot{\boldsymbol{q}}_n)$. $\widehat{(\cdot)}$ is the estimate of $(\cdot)$ under parametric uncertainties. Moreover, all configuration variables, such as $\boldsymbol{q}_n$ and $\boldsymbol{q}_r$, are in $\mathbb{R}^n$, and dynamic parameters have a compatible dimension.

The dynamics of the entire system can be expressed as

$$\boldsymbol{M}_r\ddot{\boldsymbol{q}}_r + \boldsymbol{C}_r\dot{\boldsymbol{q}}_r + \boldsymbol{g}_r = \boldsymbol{\tau}_c^{CTC}(\boldsymbol{x}_{nd}) + \boldsymbol{\tau}_a(\boldsymbol{x}_{nr}) + \boldsymbol{\tau}_{ext} \tag{10}$$

$$\widehat{\boldsymbol{M}}_n\ddot{\boldsymbol{q}}_n + \widehat{\boldsymbol{C}}_n\dot{\boldsymbol{q}}_n + \widehat{\boldsymbol{g}}_n = \boldsymbol{\tau}_c^{CTC}(\boldsymbol{x}_{nd}) - \boldsymbol{G}^T\boldsymbol{\mu}^*. \tag{11}$$

Here, similar to $(\cdot)_n$, $(\cdot)_r$ means that $(\cdot)$ is a function of the real signals. The states are defined as

$$\boldsymbol{x}_{nr} = [\boldsymbol{e}_{nr}^T, \ \dot{\boldsymbol{e}}_{nr}^T]^T, \tag{12}$$

$$\boldsymbol{x}_{nd} = [\boldsymbol{e}_{nd}^T, \ \dot{\boldsymbol{e}}_{nd}^T]^T. \tag{13}$$

The signals $\boldsymbol{q}_r$ and $\dot{\boldsymbol{q}}_r$ can be obtained from the real hardware, whereas $\boldsymbol{q}_n$ and $\dot{\boldsymbol{q}}_n$ are obtained by simulating the nominal model. Note that the actual tracking error can be obtained by $\boldsymbol{q}_r - \boldsymbol{q}_d = \boldsymbol{e}_{nd} - \boldsymbol{e}_{nr}$.

B. C-NRIC framework

In general, C-NRIC framework can employ the optimization problem (3)-(4) with the decision variable $\boldsymbol{x}$ containing at least $\ddot{\boldsymbol{q}}$. However, to simplify the explanation, let us consider the following optimization in this section.

$$\min_{\ddot{\boldsymbol{q}}} \quad \frac{1}{2}\|\ddot{\boldsymbol{q}} - \ddot{\boldsymbol{q}}_{free}\|^2_{\widehat{\boldsymbol{M}}_n}, \tag{14}$$

$$\text{subject to} \quad \boldsymbol{G}\ddot{\boldsymbol{q}} - \boldsymbol{h} \leq \boldsymbol{0}, \tag{15}$$

where

$$\ddot{\boldsymbol{q}}_{free} = \widehat{\boldsymbol{M}}_n^{-1}(\boldsymbol{\tau}_c^{CTC} - \widehat{\boldsymbol{C}}_n\dot{\boldsymbol{q}}_n - \widehat{\boldsymbol{g}}_n) \tag{16}$$

is the unconstrained acceleration of the nominal robot. With constant $\boldsymbol{G}$ and $\boldsymbol{h}$, (14)-(15) become a QP problem.

With the $\widehat{\boldsymbol{M}}_n$-weight in (14), the stationarity (5) becomes

$$\begin{aligned}\widehat{\boldsymbol{M}}_n\ddot{\boldsymbol{q}}^* + \boldsymbol{G}^T\boldsymbol{\mu}^* &= \widehat{\boldsymbol{M}}_n\ddot{\boldsymbol{q}}_{free} \\ &= \boldsymbol{\tau}_c^{CTC} - \widehat{\boldsymbol{C}}_n\dot{\boldsymbol{q}}_n - \widehat{\boldsymbol{g}}_n.\end{aligned} \tag{17}$$

Notice that this equation is equivalent to (11). It follows that we can obtain the nominal signals simply by integrating (17).

One can interpret $\boldsymbol{G}^T\boldsymbol{\mu}^*$ as a generalized force that makes the nominal robot satisfy the constraint (15). Note also that $\boldsymbol{\mu}^*$ is zero when the constraint (15) is not violated. The following theorem states the boundedness of the system states.

Theorem 1: Consider the C-NRIC framework of which structure is shown in Fig. 3. Assume that (i) the optimization (14)-(15) (or, more generally, (3)-(4)) is well-posed in the sense that there exists $\boldsymbol{x}$ such that $\boldsymbol{G}\boldsymbol{x} < \boldsymbol{h}$, (ii) $\boldsymbol{\tau}_{ext}$ is bounded, and (iii) the CTC controller in (9) is used with the PD-type auxiliary input (2). If γ is chosen sufficiently small, then the states $\boldsymbol{x}_{nr}$ and $\boldsymbol{x}_{nd}$ are bounded.

Proof: See Section IV ■

Note that the result of this theorem implies that the real robot's state is also bounded, because $\boldsymbol{q}_r - \boldsymbol{q}_d = \boldsymbol{e}_{nd} - \boldsymbol{e}_{nr}$.

[1]More formally, there exists an $\boldsymbol{x}^*$ such that $\boldsymbol{G}\boldsymbol{x}^* < \boldsymbol{h}$. This is referred to as Slater's condition.

C. Design examples

Using the C-NRIC framework, various control designs can be devised by modifying the optimization problem. In the following, we present a couple of design examples.

1) Contact-responsive motion control: A contact-responsive motion controller can be designed using the objective in (14) with the following constraint:

$$\underline{\boldsymbol{e}}_{nr} \le \boldsymbol{e}_{nr}[k+1] \le \bar{\boldsymbol{e}}_{nr}, \tag{18}$$

where $\underline{\boldsymbol{e}}_{nr}$ and $\bar{\boldsymbol{e}}_{nr}$ are known[2], and $[k]$ denotes the time index in the discrete domain. To represent (18) in the form of (15), we make the following approximation:

$$\boldsymbol{q}_n[k+1] = \boldsymbol{q}_n[k] + (\dot{\boldsymbol{q}}_n[k] + \ddot{\boldsymbol{q}}\Delta t)\,\Delta t, \tag{19}$$
$$\boldsymbol{q}_r[k+1] = \boldsymbol{q}_r[k] + \dot{\boldsymbol{q}}_r[k]\Delta t, \tag{20}$$

where Δt represents the time step. Then (18) can be rewritten as

$$\underline{\ddot{\boldsymbol{q}}} \le \ddot{\boldsymbol{q}} \le \bar{\ddot{\boldsymbol{q}}} \tag{21}$$

with

$$\begin{aligned}\underline{\ddot{\boldsymbol{q}}} =& \frac{1}{\Delta t^2}(\underline{\boldsymbol{e}}_{nr} + \boldsymbol{q}_r[k] + \dot{\boldsymbol{q}}_r[k]\Delta t - \boldsymbol{q}_n[k] - \dot{\boldsymbol{q}}_n[k]\Delta t),\\ \bar{\ddot{\boldsymbol{q}}} =& \frac{1}{\Delta t^2}(\bar{\boldsymbol{e}}_{nr} + \boldsymbol{q}_r[k] + \dot{\boldsymbol{q}}_r[k]\Delta t - \boldsymbol{q}_n[k] - \dot{\boldsymbol{q}}_n[k]\Delta t).\end{aligned} \tag{22}$$

In this formulation, $\boldsymbol{q}_n$ is forced to remain close to $\boldsymbol{q}_r$. Note that we are using PD-type robust control input $\boldsymbol{\tau}_a$ given by (2), which renders a spring-damper between $\boldsymbol{q}_n$ and $\boldsymbol{q}_r$. Therefore, only limited robustifying input $\boldsymbol{\tau}_a$ is applied to the robot, and this essentially leads to the contact-responsiveness because the robot does not try hard to overcome unknown interaction forces. In contrast, in the ordinary NRIC framework, $\boldsymbol{e}_{nr}$ can increase in the presence of the unknown interaction, and consequently, the control input $\boldsymbol{\tau}_a$ will grow to overcome the uncertainties.

2) Contact-responsive motion control with torque limiting: In this subsection, we present a more sophisticated design for the contact-responsive motion controller. To begin with, let us modify the controller (which is originally (9)) as

$$\boldsymbol{\tau}_c^{CTC\prime}(\boldsymbol{x}_{nd}) = \widehat{\boldsymbol{M}}_n(\ddot{\boldsymbol{q}}_d + (\boldsymbol{I} - diag(\boldsymbol{\lambda}))\boldsymbol{\phi}_n) + \widehat{\boldsymbol{C}}_n\dot{\boldsymbol{q}}_n + \widehat{\boldsymbol{g}}_n. \tag{23}$$

Here, $diag(\cdot)$ represents a diagonal matrix with the given values on its diagonal, and $\boldsymbol{\lambda}$ is a scaling factor that modulates $\boldsymbol{\phi}_n$.

Consider the following optimization problem:

$$\min_{\ddot{\boldsymbol{q}},\boldsymbol{\lambda}} \quad \frac{1}{2}\|\ddot{\boldsymbol{q}} - \ddot{\boldsymbol{q}}_{free} + diag(\boldsymbol{\phi}_n)\boldsymbol{\lambda}\|^2_{\widehat{\boldsymbol{M}}_n} + \frac{c}{2}\|\boldsymbol{\lambda}\|^2, \tag{24}$$
$$\text{s.t.} \quad \underline{\boldsymbol{\tau}}_a \le \boldsymbol{\tau}_a \le \bar{\boldsymbol{\tau}}_a, \tag{25}$$
$$\underline{\boldsymbol{\phi}}_n \le (\boldsymbol{I} - diag(\boldsymbol{\lambda}))\boldsymbol{\phi}_n \le \bar{\boldsymbol{\phi}}_n, \tag{26}$$

[2]For example, we can run trajectory tracking in free-motion to obtain the lower and upper bounds of $\boldsymbol{e}_{nr}$.

where $\ddot{\boldsymbol{q}}_{free}$ is defined in (16), and $\boldsymbol{\lambda}$ is an additional decision variable; hence $\boldsymbol{x} = (\ddot{\boldsymbol{q}}, \boldsymbol{\lambda})$ when written in the form of (3)-(4). The constraints can be expressed in the form of $\boldsymbol{G}\boldsymbol{x} \le \boldsymbol{h}$ using the similar approximations used in (19)-(20).

Note that $\boldsymbol{\phi}_n$ is constrained because the amount of input $\boldsymbol{\tau}_c$ may increase due to feedback error $\boldsymbol{e}_{nd}$. This happens because $\boldsymbol{q}_d$ may move far away, while $\boldsymbol{q}_n$ remains close to $\boldsymbol{q}_r$ due to the constraint (25).

Note also that $\|\boldsymbol{\lambda}\|^2$ term is introduced in the objective (24) to force the QP solver to choose small $\boldsymbol{\lambda}$ if possible. As a result, $\boldsymbol{\lambda}$ can be interpreted as a scaling factor for $\boldsymbol{\phi}_n$.

The stationarity condition (5) for this setting is

$$\begin{bmatrix}\boldsymbol{I} & diag(\boldsymbol{\phi}_n)\\ \boldsymbol{0} & c\boldsymbol{I}\end{bmatrix}\begin{bmatrix}\ddot{\boldsymbol{q}}^*\\ \boldsymbol{\lambda}^*\end{bmatrix} - \begin{bmatrix}\ddot{\boldsymbol{q}}_d\\ \boldsymbol{0}\end{bmatrix} + \begin{bmatrix}\boldsymbol{k}_v\dot{\boldsymbol{e}}_{nd} + \boldsymbol{k}_p\boldsymbol{e}_{nd}\\ \boldsymbol{0}\end{bmatrix} = -\begin{bmatrix}\widehat{\boldsymbol{M}}_n^{-1}\boldsymbol{G}_1^T & \boldsymbol{0}\\ -diag(\boldsymbol{\phi}_n)^T\boldsymbol{G}_1^T & \boldsymbol{G}_2^T\end{bmatrix}\begin{bmatrix}\boldsymbol{\mu}_1^*\\ \boldsymbol{\mu}_2^*\end{bmatrix}, \tag{27}$$

where $\boldsymbol{\mu} = [\boldsymbol{\mu}_1^T,\ \boldsymbol{\mu}_2^T]^T$ and $\boldsymbol{G} = \text{blockdiag}(\boldsymbol{G}_1, \boldsymbol{G}_2)$ are broke down with proper dimensions.

Finally, the nominal signals $\boldsymbol{q}_n$, $\dot{\boldsymbol{q}}_n$ are obtained by integrating the first row of (27). Strictly speaking, this setting does not fall into Theorem 1 because the CTC input is modified to (23). Nevertheless, the same theory can be applied with little modification as long as each component of $\boldsymbol{\lambda}^* \in [0, 1)$ which is implicitly imposed in the optimization problem (24)-(26).

IV. Theoretical derivation

The equations (10)-(11) represent the dynamics of the entire system. For the analysis purpose, instead of (10), we use so-called difference dynamics obtained by subtracting (10) from (11). After algebraic calculation, we can obtain

$$\boldsymbol{M}_r(\ddot{\boldsymbol{e}}_{nr} + \boldsymbol{L}_p\dot{\boldsymbol{e}}_{nr}) + \boldsymbol{C}_r(\dot{\boldsymbol{e}}_{nr} + \boldsymbol{L}_p\boldsymbol{e}_{nr}) = -\boldsymbol{\tau}_a(\boldsymbol{x}_{nr}) + \boldsymbol{w}, \tag{28}$$

where

$$\begin{aligned}\boldsymbol{w} =& \boldsymbol{M}_r(\widehat{\boldsymbol{M}}_n^{-1} - \boldsymbol{M}_r^{-1})(\boldsymbol{\tau}_c - \boldsymbol{G}^T\boldsymbol{\mu}^*) + \boldsymbol{M}_r\boldsymbol{L}_p\dot{\boldsymbol{e}}_{nr}\\ &+ (\boldsymbol{C}_r - \boldsymbol{M}_r\widehat{\boldsymbol{M}}_n^{-1}\widehat{\boldsymbol{C}}_n)\dot{\boldsymbol{q}}_n + \boldsymbol{C}_r\boldsymbol{L}_p\boldsymbol{e}_{nr}\\ &+ (\boldsymbol{g}_r - \boldsymbol{M}_r\widehat{\boldsymbol{M}}_n^{-1}\widehat{\boldsymbol{g}}_n) - \boldsymbol{G}^T\boldsymbol{\mu}^* - \boldsymbol{\tau}_{ext}\end{aligned} \tag{29}$$

is called extended disturbance.

To summarize, the entire system is represented by the nominal dynamics (11) and difference dynamics (28) with the states $\boldsymbol{x}_{nd}$ and $\boldsymbol{x}_{nr}$ in (12)-(13). In fact, bound of $\boldsymbol{x}_{nd}$ can be shown easily by combining converse Lyapunov theorem (e.g. Theorem 4.14 in [34]) and uniformly ultimately boundedness theory (e.g. Lemma 9.3 in [34]). Therefore, it is sufficient to investigate the boundedness of $\boldsymbol{x}_{nr}$.

The boundedness of the $\boldsymbol{x}_{nd}$ implies that $\boldsymbol{\tau}_c(\boldsymbol{x}_{nd})$ is also bounded. Under the assumption (i) that at least one feasible solution exists strictly in the constraint set, $\boldsymbol{\mu}^*$ is bounded (Theorem 2.2 in [35]).

Therefore, under the conditions (i)-(iii), the following upper bound of $\boldsymbol{w}$ can be obtained as

$$\|\boldsymbol{w}\|^2 \le c_1\|\boldsymbol{x}_{nr}\|^2 + c_2\|\boldsymbol{x}_{nr}\| + c_3, \tag{30}$$

Fig. 4. Snapshot for the experiment 1. The robot complies with the unknown obstacle obstructing the trajectory.

for some positive constant coefficients c_1, c_2, c_3. Please refer to Appendix of [25] for more details.

The difference dynamics (28) can be represented as follows in state-space.

$$\dot{\boldsymbol{x}}_{nr} = \boldsymbol{A}\boldsymbol{x}_{nr} - \boldsymbol{B}\boldsymbol{\tau}_a + \boldsymbol{B}\boldsymbol{w}, \tag{31}$$

where

$$\boldsymbol{A} = \begin{bmatrix} \boldsymbol{0} & \boldsymbol{I} \\ -\boldsymbol{M}_r^{-1}\boldsymbol{C}_r\boldsymbol{L}_p & -\boldsymbol{M}_r^{-1}\boldsymbol{C}_r - \boldsymbol{L}_p \end{bmatrix} \tag{32}$$

and $\boldsymbol{B} = [\boldsymbol{0}_{n\times n},\ \boldsymbol{M}_r^{-1}]^T$, where $\boldsymbol{0}_{n\times n}$ is a $n \times n$ matrix with zero elements.

Moreover, let us define a positive definite matrix $\boldsymbol{P}$ as

$$\boldsymbol{P} = \begin{bmatrix} \boldsymbol{L}_p\boldsymbol{M}_r\boldsymbol{L}_p + \boldsymbol{L}_p\boldsymbol{L} & \boldsymbol{L}_p\boldsymbol{M}_r \\ \boldsymbol{M}_r\boldsymbol{L}_p & \boldsymbol{M}_r \end{bmatrix}. \tag{33}$$

Then it is easy to see $\boldsymbol{B}^T\boldsymbol{P} = [\boldsymbol{L}_p,\ \boldsymbol{I}]$, and it follows that

$$\boldsymbol{\tau}_a = \boldsymbol{R}^{-1}\boldsymbol{B}^T\boldsymbol{P}\boldsymbol{x}_{nr}, \tag{34}$$

where $\boldsymbol{R} = (\boldsymbol{L} + \frac{1}{\gamma^2}\boldsymbol{I})^{-1}$. It is also interesting to observe that $\boldsymbol{P}$ satisfies

$$\dot{\boldsymbol{P}} + \boldsymbol{A}^T\boldsymbol{P} + \boldsymbol{P}\boldsymbol{A} = \begin{bmatrix} \boldsymbol{0} & \boldsymbol{L}_p\boldsymbol{L} \\ \boldsymbol{L}_p\boldsymbol{L} & \boldsymbol{0} \end{bmatrix}. \tag{35}$$

Then, it is straightforward to see that $\boldsymbol{P}$ is a solution of the following Riccati equation.

$$\dot{\boldsymbol{P}} + \boldsymbol{P}\boldsymbol{A} + \boldsymbol{A}^T\boldsymbol{P} - \boldsymbol{P}\boldsymbol{B}(\boldsymbol{R}^{-1} - \frac{1}{\gamma^2}\boldsymbol{I})\boldsymbol{B}^T\boldsymbol{P} + \boldsymbol{Q} = \boldsymbol{0}, \tag{36}$$

where $\boldsymbol{Q} = diag\{\boldsymbol{L}_p^2\boldsymbol{L},\ \boldsymbol{L}\} > \boldsymbol{0}$.

Defining $V_{nr} = \frac{1}{2}\boldsymbol{x}_{nr}^T\boldsymbol{P}\boldsymbol{x}_{nr} > 0$, its time derivative is

$$\begin{aligned} \dot{V}_{nr} =& \tfrac{1}{2}\boldsymbol{x}_{nr}^T(\dot{\boldsymbol{P}} + \boldsymbol{P}\boldsymbol{A} + \boldsymbol{A}^T\boldsymbol{P})\boldsymbol{x}_{nr} \\ & - \boldsymbol{x}_{nr}^T\boldsymbol{P}\boldsymbol{B}\boldsymbol{\tau}_a + \boldsymbol{x}_{nr}^T\boldsymbol{P}\boldsymbol{B}\boldsymbol{w}. \end{aligned} \tag{37}$$

Using (34), (36), and Young's inequality $\boldsymbol{x}_{nr}^T\boldsymbol{P}\boldsymbol{B}\boldsymbol{w} \le \frac{1}{\gamma^2}\|\boldsymbol{B}^T\boldsymbol{P}\boldsymbol{x}_{nr}\|^2 + \gamma^2\|\boldsymbol{w}\|^2$,

$$\begin{aligned} \dot{V}_{nr} &= \frac{1}{2}\boldsymbol{x}_{nr}^T(\dot{\boldsymbol{P}} + \boldsymbol{P}\boldsymbol{A} + \boldsymbol{A}^T\boldsymbol{P} - 2\boldsymbol{P}\boldsymbol{B}\boldsymbol{R}^{-1}\boldsymbol{B}^T\boldsymbol{P})\boldsymbol{x}_{nr} \\ &\quad + \boldsymbol{x}_{nr}^T\boldsymbol{P}\boldsymbol{B}\boldsymbol{w} \qquad (38) \\ &\le \tfrac{1}{2}\boldsymbol{x}_{nr}^T(\dot{\boldsymbol{P}} + \boldsymbol{P}\boldsymbol{A} + \boldsymbol{A}^T\boldsymbol{P} \\ &\quad - \boldsymbol{P}\boldsymbol{B}(\boldsymbol{R}^{-1} - \frac{1}{\gamma^2}\boldsymbol{I})\boldsymbol{B}^T\boldsymbol{P})\boldsymbol{x}_{nr} + \gamma^2\|\boldsymbol{w}\|^2 \qquad (39) \\ &\le -\lambda_m(\boldsymbol{Q})\|\boldsymbol{x}_{nr}\|^2 + \gamma^2\|\boldsymbol{w}\|^2 \qquad (40) \end{aligned}$$

where $\lambda_m(\boldsymbol{Q})$ represents the minimum eigenvalue of $\boldsymbol{Q}$.

Recall that $\|\boldsymbol{w}\|^2$ is bounded by a 2nd-order polynomial in (30). Hence it is trivial that $\|\boldsymbol{x}_{nr}\|$ is bounded in (40), as long as γ is chosen small enough to satisfy $\lambda_m(\boldsymbol{Q}) - \gamma^2 c_1 > 0$.

V. Experimental Validation

The experiments are performed using a Neuromeka Indy7 manipulator, which is a 6-dof industrial collaborative robot. We point out that Indy7 is not equipped with joint torque sensors. Namely, only joint encoders were used in the experiments. The control frequency for our setup was 2 kHz, and the qpSWIFT solver [36] was utilized for solving the QP, and its solving time was less than about 120 μs for each time step using the i7-6700k CPU. The dynamic parameters of the robot, such as mass, the center of mass, and inertia matrices, were obtained based on 3D CAD model. For all experiments, the control gains were set as $(\boldsymbol{L} + \frac{1}{\gamma^2}\boldsymbol{I}) = 132 \times \boldsymbol{I}_6$, $\boldsymbol{L}_p = diag(14, 14, 8, 8, 8, 8)$ for $\boldsymbol{\tau}_a$ in (2), and $\boldsymbol{k}_v = diag(7, 7, 5, 5, 4, 4)$, $\boldsymbol{k}_p = diag(20, 20, 14, 14, 11, 11)$ for the CTC (9).

A. Experiment1: Contact-responsive motion control with $\boldsymbol{e}_{nr}$ constraints

This section demonstrates a contact-responsive motion controller designed in Section III-C.1. In the experiment, the robot was commanded to follow a certain desired trajectory, which is obstructed by an unknown obstacle. When the robot hits the obstacle, ordinary robust control methods are not able to handle the collision safely. Indeed, when the ordinary NRIC is used, the emergency stop is activated as soon as the robot hits the obstacle, as shown in the video attachment.

In contrast, with the C-NRIC framework that can impose the constraint on $\boldsymbol{e}_{nr}$ in the form of (18) (or (21)), the robot can comply with the unknown obstacle, as shown in Fig. 4. In this experiment, the lower and upper bound of $\boldsymbol{e}_{nr}$ were $\bar{\boldsymbol{e}}_{nr} = 0.005 \times [1, 1, 1, 1, 1, 1]^T$rad, and $\underline{\boldsymbol{e}}_{nr} = -\bar{\boldsymbol{e}}_{nr}$.

Fig. 5 summarizes the experimental results. As shown in the first row, the robot follows the desired value $\boldsymbol{q}_d$ accurately in free motion. When there is a contact with the obstacle, $\boldsymbol{q}_r$ starts to deviate from $\boldsymbol{q}_d$ (see $12-17$s and $32-34$s), as expected. The second row is essentially the same, but shows the error $\boldsymbol{e}_{dr}$ instead of the joint angles. Here, it is clearly shown that the error in free motion is kept small. The third row shows that $\boldsymbol{e}_{nr}$ is bounded due to the constraint on $\boldsymbol{e}_{nr}$ (18). Finally, in the fourth row, it is shown that nonzero $\boldsymbol{G}^T\boldsymbol{\mu}^*$ occurs to ensure the constraint (18), while $\boldsymbol{\mu}^* = 0$ in free motion.

B. Experiment2: Contact-responsive motion control with torque limiting constraints

As presented in Section III-C.2, we can design a more sophisticated contact-responsive motion controller by imposing

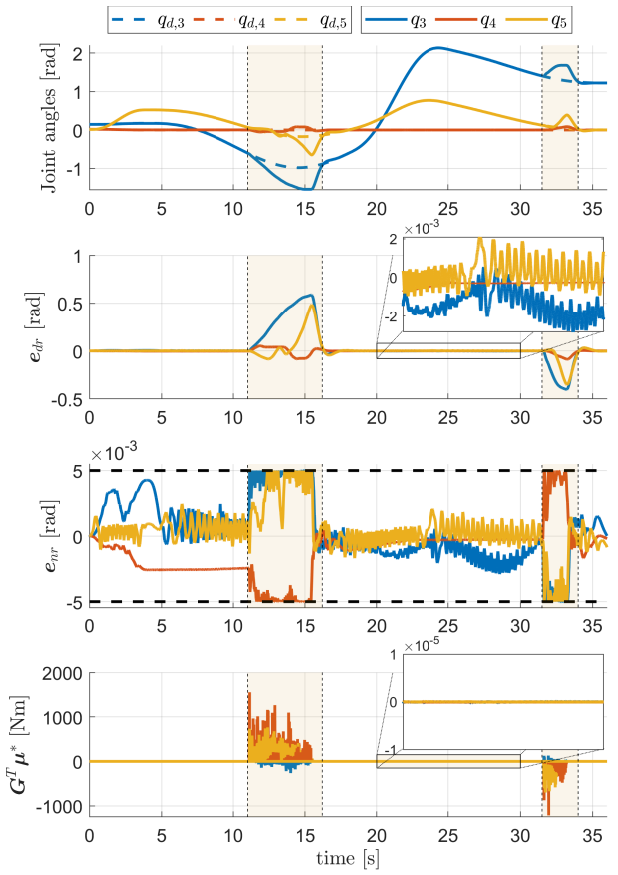

Fig. 5. Results of the experiment1. In the first row, dashed and solid lines represent the desired and real positions, respectively. The small boxes in the second and fourth rows magnify the plot for the time interval of 20-30s, during which the robot is in free motion. The plots display only the 3rd, 4th, and 5th joints to improve readability.

constraints on $\boldsymbol{\tau}_a$ and $\boldsymbol{\phi}_n$. We report that, with this setting, the robot can behave very similar to the previous experiment, in which only $\boldsymbol{e}_{nr}$ is constrained. Due to space constraints in the manuscript, we instead present another experiment that demonstrates the effectiveness of the torque limiting.

In this experiment, we make the robot follow a trajectory consists of upward and downward motions. As shown in Fig. 6, the robot tracks the upward trajectory in free motion. In contrast, during the downward trajectory, we put an egg below the robot to make a contact. By limiting the $\boldsymbol{\tau}_a$ and $\boldsymbol{\phi}_n$ properly, it is expected that the robot does not break the egg. To this end, the constraints (25)-(26) were set using $\bar{\boldsymbol{\tau}}_a = [18, 18, 8, 8, 2, 2]^T \mathrm{Nm}$, $\bar{\boldsymbol{\phi}}_n = 0.2 \times [1, 1, 1, 1, 2, 2]^T \mathrm{rad/s^2}$, $\underline{\boldsymbol{\tau}}_a = -\bar{\boldsymbol{\tau}}_a$, and $\underline{\boldsymbol{\phi}}_n = -\bar{\boldsymbol{\phi}}_n$.

Fig. 7 shows the experimental results. The first row shows that the robot tracks the desired value at the beginning, whereas it is blocked by the egg during the downward trajectory. The second row shows the bound of $\boldsymbol{\tau}_a$. Similarly, the third row shows the bound of $\boldsymbol{\phi}_n$ with the scaling factor $\boldsymbol{\lambda}$ on the fourth row.

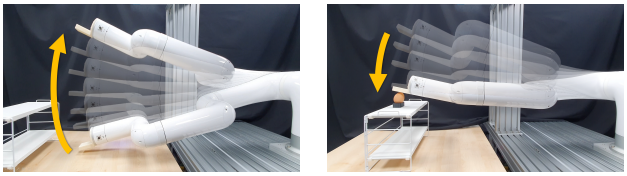

(a) (b)

Fig. 6. Setup for the experiment2.

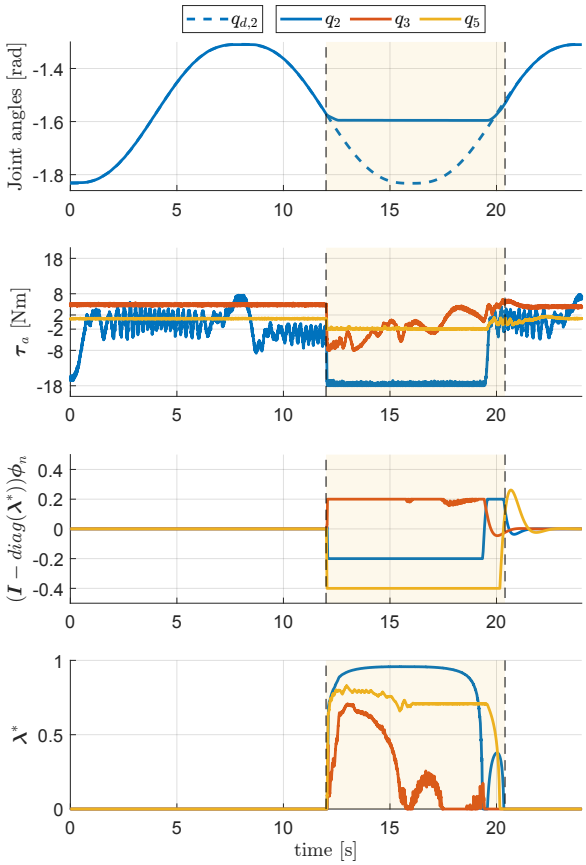

Fig. 7. Results of the experiment2. In the first row, dashed and solid lines represent the desired and real positions, respectively. The plots display only the 2nd, 3rd, and 5th joints to improve readability. The top row shows the 2nd joint exclusively for the same purpose.

VI. Conclusion

In this paper, we presented a method of imposing constraints on the NRIC framework, which is a class of nonlinear DOB. For this reason, the proposed method is called constrained NRIC (C-NRIC) framework. As long as the constraints are well-posed in the sense that a feasible solution exists strictly in the constraint set, the system states are bounded (Theorem 1). As an application of the C-NRIC framework, we presented a couple of contact-responsive motion control designs. Conceptually speaking, such controllers can be realized by updating the nominal robot in such a way that the nominal signal does not deviate too much from the real robot. Consequently, the robot could comply with the interaction force caused by unknown obstacles. The proposed scheme was validated through the real-world experiments.

REFERENCES

[1] G. Garofalo, N. Mansfeld, J. Jankowski, and C. Ott, "Sliding mode momentum observers for estimation of external torques and joint acceleration," in *2019 International Conference on Robotics and Automation (ICRA)*. IEEE, 2019, pp. 6117–6123.

[2] W. Jie, Z. Yudong, B. Yulong, H. H. Kim, and M. C. Lee, "Trajectory tracking control using fractional-order terminal sliding mode control with sliding perturbation observer for a 7-dof robot manipulator," *IEEE/ASME Transactions on Mechatronics*, vol. 25, no. 4, pp. 1886–1893, 2020.

[3] R. Ortega, V. Nikiforov, and D. Gerasimov, "On modified parameter estimators for identification and adaptive control. a unified framework and some new schemes," *Annual Reviews in Control*, vol. 50, pp. 278–293, 2020.

[4] X. Wu, A. Kirner, G. Garofalo, C. Ott, P. Kotyczka, and A. Dietrich, "Adaptive tracking control with uncertainty-aware and state-dependent feedback action blending for robot manipulators," *IEEE Robotics and Automation Letters*, vol. 7, no. 4, pp. 12 307–12 314, 2022.

[5] Y. Choi, W. K. Chung, and I. H. Suh, "Performance and h/sub/spl infin//optimality of pid trajectory tracking controller for lagrangian systems," *IEEE Transactions on Robotics and Automation*, vol. 17, no. 6, pp. 857–869, 2001.

[6] D. Larby and F. Forni, "A passivity preserving h-infinity synthesis technique for robot control," in *IEEE 61st Conference on Decision and Control (CDC)*, 2022, pp. 1416–1422.

[7] M. J. Kim, A. Werner, F. Loeffl, and C. Ott, "Passive impedance control of robots with viscoelastic joints via inner-loop torque control," *IEEE Transactions on Robotics*, vol. 38, no. 1, pp. 584–598, 2021.

[8] J. Jeong and M. J. Kim, "Passivity-based decentralized control for collaborative grasping of under-actuated aerial manipulators," in *2023 IEEE International Conference on Robotics and Automation (ICRA)*, 2023, pp. 7699–7705.

[9] C. E. Garcia and M. Morari, "Internal model control. a unifying review and some new results," *Industrial & Engineering Chemistry Process Design and Development*, vol. 21, no. 2, pp. 308–323, 1982.

[10] S. P. Karason and A. M. Annaswamy, "Adaptive control in the presence of input constraints," in *1993 american control conference*. IEEE, 1993, pp. 1370–1374.

[11] G. Wredenhagen and P. Belanger, "Piecewise-linear LQ control for systems with input constraints," *Automatica*, vol. 30, no. 3, pp. 403–416, 1994.

[12] D. Q. Mayne, J. B. Rawlings, C. V. Rao, and P. O. Scokaert, "Constrained model predictive control: Stability and optimality," *Automatica*, vol. 36, no. 6, pp. 789–814, 2000.

[13] P. J. Goulart, E. C. Kerrigan, and J. M. Maciejowski, "Optimization over state feedback policies for robust control with constraints," *Automatica*, vol. 42, no. 4, pp. 523–533, 2006.

[14] T. Howard, M. Pivtoraiko, R. A. Knepper, and A. Kelly, "Model-predictive motion planning: Several key developments for autonomous mobile robots," *IEEE Robotics & Automation Magazine*, vol. 21, no. 1, pp. 64–73, 2014.

[15] C. E. Luis, M. Vukosavljev, and A. P. Schoellig, "Online trajectory generation with distributed model predictive control for multi-robot motion planning," *IEEE Robotics and Automation Letters*, vol. 5, no. 2, pp. 604–611, 2020.

[16] S. Kleff, A. Meduri, R. Budhiraja, N. Mansard, and L. Righetti, "High-frequency nonlinear model predictive control of a manipulator," in *2021 IEEE International Conference on Robotics and Automation (ICRA)*. IEEE, 2021, pp. 7330–7336.

[17] Y. Ding, A. Pandala, C. Li, Y.-H. Shin, and H.-W. Park, "Representation-free model predictive control for dynamic motions in quadrupeds," *IEEE Transactions on Robotics*, vol. 37, no. 4, pp. 1154–1171, 2021.

[18] M. Rauscher, M. Kimmel, and S. Hirche, "Constrained robot control using control barrier functions," in *2016 IEEE/RSJ International Conference on Intelligent Robots and Systems (IROS)*. IEEE, 2016, pp. 279–285.

[19] D. Lee, D. Ko, W. K. Chung, and K. Kim, "Quadratic programming-based task scaling for safe and passive robot arm teleoperation," *IEEE/ASME Transactions on Mechatronics*, vol. 27, no. 4, pp. 1937–1945, 2022.

[20] F. Ferraguti, C. T. Landi, A. Singletary, H.-C. Lin, A. Ames, C. Secchi, and M. Bonfè, "Safety and efficiency in robotics: the control barrier functions approach," *IEEE Robotics & Automation Magazine*, vol. 29, no. 3, pp. 139–151, 2022.

[21] S. Oh, H. Woo, and K. Kong, "Frequency-shaped impedance control for safe human–robot interaction in reference tracking application," *IEEE/ASME Transactions On Mechatronics*, vol. 19, no. 6, pp. 1907–1916, 2014.

[22] E. Sariyildiz, R. Oboe, and K. Ohnishi, "Disturbance observer-based robust control and its applications: 35th anniversary overview," *IEEE Transactions on Industrial Electronics*, vol. 67, no. 3, pp. 2042–2053, 2019.

[23] K. Samuel, K. Haninger, S. Oh, and C. Lee, "Reduced-order nominal model design and validation for task space DOB-based motion control of an industrial robot," in *2023 IEEE/ASME International Conference on Advanced Intelligent Mechatronics (AIM)*. IEEE, 2023, pp. 1095–1101.

[24] B. K. Kim, H.-T. Choi, W. K. Chung, and I. H. Suh, "Analysis and design of robust motion controllers in the unified framework," *J. Dyn. Sys., Meas., Control*, vol. 124, no. 2, pp. 313–321, 2002.

[25] M. J. Kim, Y. Choi, and W. K. Chung, "Bringing nonlinear $\mathcal{H}_\infty$ optimality to robot controllers," *IEEE Transactions on Robotics*, vol. 31, no. 3, pp. 682–698, 2015.

[26] M. J. Kim, Y. J. Park, and W. K. Chung, "Design of a momentum-based disturbance observer for rigid and flexible joint robots," *Intelligent Service Robotics*, vol. 8, pp. 57–65, 2015.

[27] M. J. Kim, F. Beck, C. Ott, and A. Albu-Schäffer, "Model-free friction observers for flexible joint robots with torque measurements," *IEEE Transactions on Robotics*, vol. 35, no. 6, pp. 1508–1515, 2019.

[28] D. Ko, D. Lee, W. K. Chung, and K. Kim, "Bounded compensation with friction estimation for accurate motion tracking and compliant behavior of industrial manipulators," in *2023 IEEE International Conference on Robotics and Automation (ICRA)*. IEEE, 2023, pp. 5235–5241.

[29] W.-H. Chen, D. J. Ballance, P. J. Gawthrop, and J. O'Reilly, "A nonlinear disturbance observer for robotic manipulators," *IEEE Transactions on industrial Electronics*, vol. 47, no. 4, pp. 932–938, 2000.

[30] W. Lee, M. J. Kim, and W. K. Chung, "Asymptotically stable disturbance observer-based compliance control of electrohydrostatic actuators," *IEEE/ASME Transactions on Mechatronics*, vol. 25, no. 1, pp. 195–206, 2019.

[31] S. Haddadin, A. De Luca, and A. Albu-Schäffer, "Robot collisions: A survey on detection, isolation, and identification," *IEEE Transactions on Robotics*, vol. 33, no. 6, pp. 1292–1312, 2017.

[32] S. W. Han and M. J. Kim, "Proprioceptive sensor-based simultaneous multi-contact point localization and force identification for robotic arms," in *2023 IEEE International Conference on Robotics and Automation (ICRA)*, 2023, pp. 12 099–12 105.

[33] S. Boyd, S. P. Boyd, and L. Vandenberghe, *Convex optimization*. Cambridge university press, 2004.

[34] H. K. Khalil, *Nonlinear Systems*, 3rd ed. Englewood Cliffs, NJ: Prentice-Hall, 2002.

[35] J. Gauvin and J. W. Tolle, "Differential stability in nonlinear programming," *SIAM Journal on Control and Optimization*, vol. 15, no. 2, pp. 294–311, 1977.

[36] A. G. Pandala, Y. Ding, and H.-W. Park, "qpSWIFT: A real-time sparse quadratic program solver for robotic applications," *IEEE Robotics and Automation Letters*, vol. 4, no. 4, pp. 3355–3362, 2019.